PHYSICAL REVIEW B **96**, 041121(R) (2017)

Two-dimensional electron systems in ATiO$_3$ perovskites (A=Ca, Ba, Sr): Control of orbital hybridization and energy order

T. C. Rödel,[1,2,*] M. Vivek,[3] F. Fortuna,[1] P. Le Fèvre,[2] F. Bertran,[2] R. Weht,[4,5] J. Goniakowski,[6] M. Gabay,[3] and A. F. Santander-Syro[1,†]

[1]*CSNSM, Univ. Paris-Sud, CNRS/IN2P3, Université Paris-Saclay, 91405 Orsay Cedex, France*

[2]*Synchrotron SOLEIL, L'Orme des Merisiers, Saint-Aubin-BP48, 91192 Gif-sur-Yvette, France*

[3]*Laboratoire de Physique des Solides, CNRS, Univ. Paris-Sud, Université Paris-Saclay, 91405 Orsay Cedex, France*

[4]*Gerencia de Investigación y Aplicaciones, Comisión Nacional de Energía Atómica, Avenida General Paz y Constituyentes, 1650 San Martín, Argentina*

[5]*Consejo Nacional de Investigaciones Científicas y Técnicas (CONICET), C1425FQB Buenos Aires, Argentina*

[6]*Institut des NanoSciences de Paris, CNRS and Sorbonne Universités, UPMC Univ. Paris 06, UMR 7588, F-75005 Paris, France*

(Received 6 March 2017; published 21 July 2017)

We report the existence of a two-dimensional electron system (2DES) at the (001) surface of CaTiO$_3$. Using angle-resolved photoemission spectroscopy, we find a hybridization between the d_{xz} and d_{yz} orbitals, not observed in the 2DESs at the surfaces of other ATiO$_3$ perovskites, e.g., SrTiO$_3$ or BaTiO$_3$. Based on a comparison of the 2DES properties in these three materials, we show how the electronic structure of the 2DES (bandwidth, orbital energy order, and electron density) is coupled to different typical lattice distortions in perovskites. The orbital hybridization in orthorhombic CaTiO$_3$ results from the rotation of the oxygen octahedra, which can also occur at the interface of oxide heterostructures to compensate strain. More generally, the control of the orbital energy order in 2DES by choosing different A-site cations in perovskites offers a gateway toward 2DESs in oxide heterostructures beyond SrTiO$_3$.

DOI: 10.1103/PhysRevB.96.041121

Introduction. ABO_3 perovskites, where B is a transition-metal ion, present many appealing phenomena, including ferroelectricity, ferromagnetism, superconductivity, and strong electron correlations [1,2]. One reason for such a diversity is that the perovskite lattice can accommodate a large variety of differently sized A and B cations as described by Goldschmidt's tolerance factor [3]. This factor can be widely varied by the size of the A-site cation, resulting in different lattice distortions which strongly influence the electronic structure [4,5].

Such a variety of functionalities within the same oxide family, together with the epitaxial compatibility amongst many of its members, has boosted the interest in oxide heterostructures over the last two decades. One prime example of these emerging properties is the two-dimensional electron system (2DES) found at the LaAlO$_3$/SrTiO$_3$ interface [6], which shows a wide range of properties including the coexistence of superconductivity and magnetism [7,8] as well as a possibly unusual electron pairing mechanism [9]. More recently, the discoveries of 2DESs at bare surfaces of various perovskites such as the paraelectric SrTiO$_3$ [10–14], the strong spin-orbit coupled KTaO$_3$ [15–17], the catalyst TiO$_2$ anatase [18], or the ferroelectric BaTiO$_3$ [19] triggered new avenues of research by providing deep insight into the microscopic electronic structure of such 2DESs, including orbital energy order, symmetries, and electron-phonon interaction effects [10,11,20,21].

Here we report the discovery of a 2DES at the (001) surface of CaTiO$_3$. Moreover we find a significant hybridization between the d_{xz} and d_{yz} orbitals forming the 2DES, not observed in the 2DESs at the surface of other perovskite titanates, and show that it is induced by the rotation of the oxygen octahedra in the orthorhombic lattice resulting from the small size of the Ca ion. This is very appealing, as the possibility to use octahedral tilts to control the properties of oxide interfaces, such as magnetism, has attracted much attention lately [22–24]. To further explore the connection between lattice distortions in the perovskites and electronic structures in 2DES, we compare the 2DESs measured by ARPES at the surface of different titanates, ATiO$_3$ (A = Ca, Sr, Ba) [19]. We thus show that the bandwidths, the order of the orbital energies, and the orbital symmetries (hybridization between different orbital characters) all depend on the size of the A-site cation.

Methods. The angle-resolved photoemission spectroscopy (ARPES) measurements were conducted at the Synchrotron Radiation Center (University of Wisconsin, Madison) and the CASSIOPEE beamline of Synchrotron Soleil (France) at temperatures T = 7–20 K and pressures lower than $P = 6 \times 10^{-11}$ Torr. Details on the surface preparation and creation of the 2DES are discussed in the Supplemental Material [25]. Density Functional Theory (DFT) calculations were carried out on bulk CaTiO$_3$. Values of the lattice parameters, tilt angles, and band gaps were estimated and compared to experimental data reported in [26]. Of the three exchange-correlation functionals tested, the hybrid one (HSE06) gave the best agreement with the experimental values (see Supplemental

*Present address: Laboratory for Photovoltaics, Physics and Material Science Research Unit, University of Luxembourg, L-4422 Belvaux, Luxembourg.

†andres.santander@csnsm.in2p3.fr

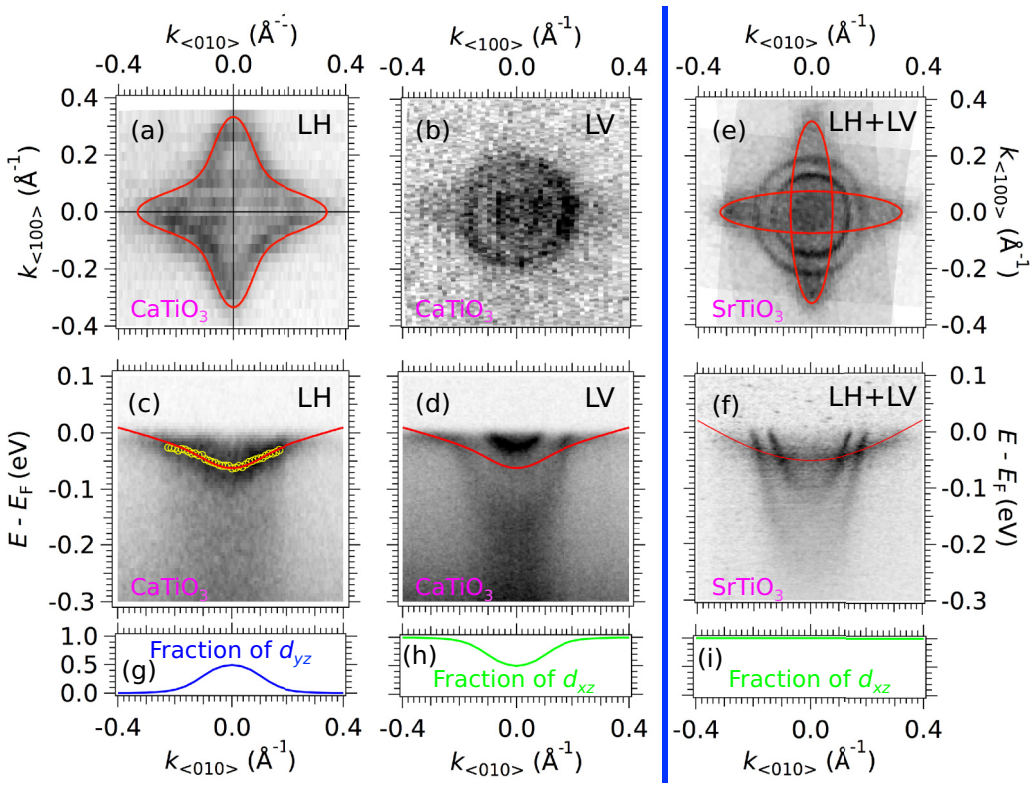

FIG. 1. (a), (b) Fermi surface intensity maps of the 2DES measured at the surface of $CaTiO_3$(001) close to $\Gamma_{005}(h\nu = 57$ eV) using LH polarization, and close to $\Gamma_{115}(h\nu = 67$ eV) using LV polarization, respectively. (c), (d) $E - k$ intensity maps measured at Γ_{005} using LH and LV polarization. The red curves are based on a one-layer tight-binding model assuming orbital hybridization between the d_{xz} and d_{yz} orbitals. The yellow markers in (c) are the peak positions of the fits of the energy distribution curves (EDCs). (e), (f) Fermi surface and $E - k$ map corresponding to the electronic structure of the 2DES at the (001) surface of $SrTiO_3$. The shown intensity maps are a superposition of measurements using LH polarization at $h\nu = 90$ eV and LV polarization at $h\nu = 47$ eV. The red curves are, in this case, based on a tight-binding model *without* hybridization between the different t_{2g} orbitals. (g)–(i) Momentum-resolved fraction of orbital character of the d_{xz} or d_{yz} band visible in the $E - k$ maps in (c), (d), and (f) based on the tight-binding model showing the orbital hybridization in the 2DES at the (001) surface of $CaTiO_3$.

Material [25] for a comparison of the results obtained with different functionals). With this choice, the calculated lattice parameters differ from the experimental estimates by less than 0.01 Å and the tilt angles by less than 0.2°. The band gap is estimated to be 3.62 eV as compared to the experimental value of 3.50 eV [27]. All through this Rapid Communication, directions and planes are defined in the quasicubic cell of $CaTiO_3$. In this way, the (x, y, z) axes used to express orbitals and wave functions are defined along the Ti-O-Ti directions. In contrast, for experimental convenience, the indices h, k, and l of Γ_{hkl} correspond to the reciprocal lattice vectors of the orthorhombic unit cell.

Experimental results. Figures 1(a) and 1(b) show the different observed Fermi surfaces in the (001) plane of pseudocubic $CaTiO_3$. They were measured, respectively, around Γ_{005} using $h\nu = 57$ eV photons with linear vertical (LV) polarization, and around Γ_{115} using $h\nu = 67$ eV photons with linear horizontal (LH) polarization. One Fermi sheet consists of a four-pointed star as shown in Fig. 1(a), while two other Fermi sheets are circular as seen in Fig. 1(b). Figures 1(c) and 1(d) present the energy-momentum maps close to the bulk Γ_{005} point along the ⟨010⟩ direction, using, respectively, LH and LV polarizations. In Fig. 1(d) one observes two dispersive light bands and a portion of the heavy band close to the Fermi level, whereas the other part of the heavy band, with the bottom about 62 meV below E_F, can be seen in Fig. 1(c).

To understand the originality of the 2DES in $CaTiO_3$, it is instructive to compare its electronic structure with that found in $SrTiO_3$. Figures 1(e) and 1(f) show, respectively, the Fermi surface and $E - k$ map obtained at the Al-capped $SrTiO_3$(001) surface—-a protocol recently developed by us to create highly homogeneous 2DES on several oxides [19]. We thus identify three bands, two light and one heavy, in the $E - k$ maps of both materials. In $SrTiO_3$, the two light bands have d_{xy} character, while the heavy band has d_{yz} (d_{xz}) character along k_x (k_y) [10,11]. For $CaTiO_3$, as will be fully justified by our DFT calculations below, we also identify the subbands as states of the t_{2g} manifold. The two light bands correspond to d_{xy} bands forming circular Fermi surface sheets (see the Supplemental Material [25] for additional data close to Γ_{005} and Γ_{115}, as well as photon energy dependence of ARPES data in $CaTiO_3$, to confirm their orbital and 2D characters). However, the dispersion of the heavy band is clearly different in $SrTiO_3$ and $CaTiO_3$. The rotation of the oxygen octahedra in $CaTiO_3$ breaks the cubic symmetry of the ideal perovskite lattice ($SrTiO_3$) and thus can result in the hybridization of orbitals

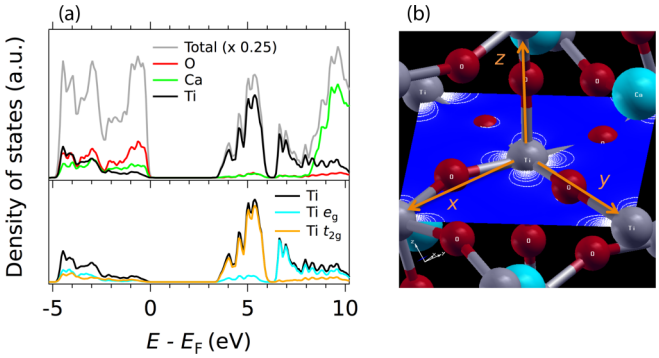

FIG. 2. (a) Top: Total, Ti-, Ca-, and O-projected densities of states of bulk $CaTiO_3$ obtained from DFT − HSE06 calculations. Bottom: Decompositions into Ti e_g ($d_{z^2} + d_{x^2-y^2}$) and Ti t_{2g} ($d_{xy} + d_{yz} + d_{xz}$) components shows that the conduction band minimum of $CaTiO_3$ is mainly formed of t_{2g} orbitals (see details in the DFT section of the Supplemental Material [25]). (b) Cut into the pseudo-TiO_2 plane (blue plane) of the charge density plot (white contours) for the lower-energy state of the conduction band in $CaTiO_3$. Ca, Ti, and O atoms are represented by cyan, gray, and red spheres, respectively. Orange arrows show the (x,y,z) axes of the pseudocubic unit cell.

of different azimuthal quantum numbers. The hybridization of the d_{xz} and d_{yz} bands in $CaTiO_3$ is evident from the star-shaped Fermi surface in Fig. 1(a), which can be understood as resulting from the hybridization of the two elliptic Fermi surface sheets in Fig. 1(e), and is further supported by the nonparabolic dispersion as well as the light polarization dependence of the heavy band in Figs. 1(c) and 1(d). In fact, the dispersions of the heavy subbands in $CaTiO_3$ can be fitted using a minimal one-layer tight-binding model assuming hybridization of the d_{xz} and d_{yz} bands, as shown by the red curves in Figs. 1(a), 1(c) and 1(d). Based on such model, Figs. 1(g)–1(i) show the momentum-resolved fraction of the orbital character of the hybrid heavy band, demonstrating the hybridization between the d_{xz} and d_{yz} orbitals in $CaTiO_3$, and the pure d_{xz} orbital character of the heavy band in $SrTiO_3$. Details on the used tight-binding model are provided in the Supplemental Material [25].

From Figs. 1(c) and 1(d), the bottoms of the d_{xy} subbands at the surface of $CaTiO_3$ are located at −158 meV and −27 meV, while the bottom of the hybrid (d_{xz},d_{yz}) heavy subband is at −62 meV. Parabolic fits around Γ yield an effective mass of approximately $m_{d_{xy}} = 1.1m_e$ for the d_{xy} bands, and $m_{d_{xz,yz}}(\Gamma) = 2.7m_e$ for the heavy band. Based on the tight-binding model described before, the mass of the heavy band sufficiently away from Γ (close to its Fermi momenta k_F, where orbital hybridization is negligibly small) is $m_{d_{xz,yz}}(k_F) \approx 15m_e$. The Fermi momenta of the d_{xy} subbands are 0.07 and 0.20 $Å^{-1}$, and 0.38 $Å^{-1}$ for the hybrid heavy subband. This gives an electron concentration of $n_{2D} \approx 1.2 \times 10^{14}$ cm^{-2}, or about 0.17 electrons per a^2, where a is the pseudocubic lattice constant of the orthorhombic lattice.

Numerical calculations. We carried out DFT calculations to understand how the rotation of the oxygen octahedra surrounding the Ti^{4+} cation, and the concomitant altered bonding angle Ti-O-Ti, affect the energy order of the crystal field split t_{2g} (d_{xy},d_{yz},d_{xz}) and e_g (d_{z^2},$d_{x^2-y^2}$) orbitals in bulk $CaTiO_3$. In fact, as shown by the projected densities of states in Fig. 2(a), top panel, the top of the valence band (set as zero of energy) has mostly oxygen character, while Ti states contribute mainly to the bottom of the conduction band (CB). Moreover, as demonstrated in Fig. 2(a), bottom panel, a decomposition into Ti e_g and t_{2g} components shows that the CB minimum displays predominantly a t_{2g} character, consistent with the octahedral environment of Ti cations. Thus, despite the non-negligible tilt of the TiO_6 octahedra in the bulk $CaTiO_3$ structure, the contribution of the e_g component to the bottom of the CB is small, and it totally vanishes at the CB minimum at Γ. In fact, as shown in Fig. 2(b), the projection of the lower-energy conduction state into the experimentally studied pseudo-TiO_2 plane shows clearly that the electron wave function in this plane presents the symmetry of t_{2g} orbitals. Thus, the 2DES at the (001) surface of $CaTiO_3$ should be mainly composed of the t_{2g} states, which justifies the choice of tight-binding orbitals used to fit the experimental data in Fig. 1.

Indeed, note from Figs. 1(a)–1(d) that such minimal tight-binding model explains very well the measured band dispersions and Fermi surface. This implies that filling of the bulk conduction band plus confinement on the surface are the main ingredients needed to explain the observed 2DES, and additional surface-induced modifications of the crystal structure, if present, play a secondary role.

The Supplemental Material [25] presents a detailed description of our DFT calculations.

Comparison between various ATiO$_3$ perovskites. The 2DES at the surface of $CaTiO_3$, presented in this Rapid Communication, is a new member of the family of $ATiO_3$ perovskites hosting a 2DES on its surface ($SrTiO_3$ and $BaTiO_3$) [10,19]. The comparison of these 2DESs gives insight into the coupling of the electronic structure to different lattice symmetries, as the three oxides show fundamentally different lattice distortions. While $SrTiO_3$ is (close to) the perfect cubic perovskite structure, the oxygen octahedra are rotated in $CaTiO_3$, and in $BaTiO_3$ the Ti cation moves away from the center of the octahedra resulting in a ferroelectric distortion. These rotations/distortions and the corresponding electronic structure of the 2DESs, based on our ARPES measurements, are schematized in Figs. 3(a)–3(c). The ARPES results on the 2DESs are also summarized in Table I. The differences in the electron structure will be discussed in the next paragraphs.

The effective mass of the d_{xy} subbands is larger by a factor of 1.6 in $CaTiO_3$ compared to $SrTiO_3$, due to the rotation-induced decrease in the Ti d bandwidth [28]. This reduced bandwidth or, respectively, increased density of states was related to a more robust ferromagnetism at the $LaAlO_3/CaTiO_3$ interface compared to the $LaAlO_3/SrTiO_3$ interface, although the driving force for the magnetic order is the d_{xz} and d_{yz}, not the d_{xy}, orbitals [23]. Due to the orbital hybridization of the d_{xz} and d_{yz} bands, $m^*_{d_{xz,yz}}$ is about five times smaller close to Γ than far away from Γ (near E_F) in $CaTiO_3$. These insights are also of relevance for $SrTiO_3$-based heterostructures, as rotations of octahedra can occur at interfaces [28–30].

While the electron densities are rather similar in $CaTiO_3$ and $SrTiO_3$ (factor of 1.2), n_{2D} in $BaTiO_3$ is at least twice as large compared to the other oxides. The ferroelectric polarization

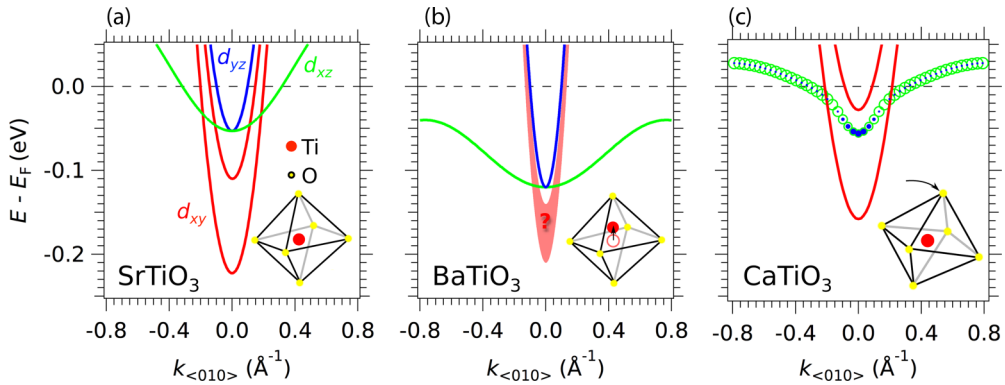

FIG. 3. Oxygen octahedra in $ATiO_3$ (A = Sr, Ba, Ca) perovskites and schematic of band dispersion observed in the 2DESs in $SrTiO_3$ (a), $BaTiO_3$ (b), and $CaTiO_3$ (c). The black arrows in (b) and (c) indicate the distortion occurring in $BaTiO_3$ and $CaTiO_3$. The broad red band and the question mark in (b) indicate that the band structure of the d_{xy} band was not resolved well by ARPES in $BaTiO_3$. The colors of the bands correspond to different orbital characters. The size of the blue filled and green empty circles in (c) represents the fraction of the d_{xz} (green) and the d_{yz} (blue) in the band dispersion.

in single domain $BaTiO_3/SrTiO_3$ thin films is in the upward direction, i.e., toward the surface [31]. The resulting electric field will influence the confining field of the 2DES and thus, the electron density can be altered. Hence, in principle, n_{2D} can be controlled by the polarization in the thin film which can be manipulated by choosing different substrates [31] or by applying strain gradients [32].

TABLE I. Relationships between crystal structure and electronic properties of the 2DES at the surface of $CaTiO_3$, $SrTiO_3$, and $BaTiO_3$. The Goldschmidt's tolerance factor and the lattice symmetry are given in the first two rows. The effective masses $m^\star$ (in units of the free electron mass m_e) of the d_{xy} and d_{xz},d_{yz} bands are given in the next two rows. The subsequent four rows give the bottom energies of the t_{2g} bands ($E_{t_{2g}}$) together with the energy difference between the two d_{xy} subbands, $\Delta E_{d_{xy}}$. The ninth row specifies the observed order of orbital energies. The last row gives the electron density n_{2D} of the 2DES. All data correspond to the maximal electron density observed for each of the 2DESs.

	$CaTiO_3$	$SrTiO_3$ [19]	$BaTiO_3$ [19]
Tolerance	0.97	1.01	1.08
Phase at RT	Orthorhombic	Cubic	Tetragonal
$m^\star_{d_{xy}}/m_e$	1.1	0.7	0.3 ± 0.2[a]
$m^\star_{d_{xz/yz}}/m_e$	2.7 at Γ	7 ± 1	10 ± 2
$E^{(1)}_{d_{xy}}$ (meV)	158	223	200 ± 60[a]
$E^{(2)}_{d_{xy}}$ (meV)	27	110	
$\Delta E_{d_{xy}}$ (meV)	131	113	
$E_{d_{xz/yz}}$ (meV)	62	50	135 ± 10
Orbital energy order	xy,(xz/yz),xy	xy,xy,xz/yz	xy,xz/yz
n_{2D} (10^{14} cm^{-2})	1.2	1.4	2.8 ± 0.4

[a]The dispersion of the light d_{xy} band in $BaTiO_3$ has not been resolved well by ARPES. The light electron mass $m^\star_{d_{xy}}$ is estimated from the band bottom and Fermi momenta of the d_{xz} or d_{yz} band along the "light" direction (x for d_{xz}, y for d_{yz}). The band bottom $E^{(1)}_{d_{xy}}$ in $BaTiO_3$ is estimated from the peak in the EDC at Γ (Supplemental Material [25]).

The order of the orbital energies in 2DESs is mainly determined by the effective mass along the confinement direction m^*_z [10]. As shown previously, the orbital mixing in $CaTiO_3$ influences $m^*_{d_{xz,yz}}$ in the surface plane, and will also influence m^*_z for this band. Thus, the combined effects of hybridization and electron confinement determine the hierarchy or orbital energies. Consequently, as seen in Fig. 3 and summarized in Table I, the hybridized band in $CaTiO_3$ is *in between* two d_{xy} subbands, in contrast to the d_{xy}-d_{xy}-$d_{xz/yz}$ energy order in $SrTiO_3$ [10,19].

The ordering of orbital energies in the 2DES at the $LaAlO_3/SrTiO_3$ interface is essential to understand its properties. Many of the unusual phenomena at this interface are related to the Lifshitz transition occurring at electron densities at which the heavy bands d_{xz}/d_{yz} start to be populated [33–35]. In contrast, other phenomena are only observed in pure d_{xy} systems, e.g., the quantum Hall effect [36]. In $SrTiO_3$-based interfaces the control of the orbital energy order and occupancy is based on adjusting the electron density and the spatial extension as well as depth of the quantum well confining the electrons, depending, for example, on the composition of the oxide heterostructure [36]. Another way is to choose different surface or interface orientations in $SrTiO_3$ [13,37]. The present study demonstrates another possibility by choosing different A-site cations in the perovskite lattice. New insights into the properties at the interfaces of complex oxides could be gained by studying Lifshitz transition in 2DESs in $CaTiO_3$ and $BaTiO_3$.

Conclusions. We studied the coupling between the lattice structure and the electronic structure of 2DES at the surface of three different insulating perovskites $ATiO_3$. Our reference system is the 2DES in cubic $SrTiO_3$ which has been intensively studied at its bare surface as well as at the $LaAlO_3/SrTiO_3$ interface. The orthorhombic distortions in $CaTiO_3$ result in a hybridization of the d_{xz} and d_{yz} orbitals. The ferroelectric distortions in $BaTiO_3$ result in a macroscopic polarization which influences the electron density of the 2DES. Moreover, the distortions change bandwidth as well as the energy order of the t_{2g} manifold in the 2DES. Both bandwidth and order of orbital energies influence the macroscopic, e.g., magnetic

and transport, properties of the 2DESs [23,34]. Our results motivate the study of interfaces beyond $SrTiO_3$ as so far the question of whether the properties of the $LaAlO_3/SrTiO_3$ interface can be generalized to 2DES in other perovskite oxides remains largely unanswered.

Note added. Recently, we learned of a related work [53].

Acknowledgments. We thank Cédric Baumier for help during ARPES experiments, and Marcelo Rozenberg for discussions. This work was supported by public grants from the Agence Nationale de la Recherche (ANR, France), project LACUNES No. ANR-13-BS04-0006-01, the "Laboratoire d'Excellence Physique Atomes Lumière Matière" (LabEx PALM projects ELECTROX and 2DEGS2USE) overseen by the ANR as part of the "Investissements d'Avenir" program (reference: ANR-10-LABX-0039), and the CNRS-CONICET 2015-2016 collaborative project AMODOX (project No. 254274). T.C.R. acknowledges funding from the RTRA–Triangle de la Physique (project PEGASOS). R.W. acknowledges support from CONICET (Grant No. PIP 114-201101-00376) and ANPCyT (Grant No. PICT-2012-0609). M.G. and A.F.S.-S. acknowledge the support received from the Institut Universitaire de France.

[1] E. Dagotto and Y. Tokura, MRS Bull. **33**, 1037 (2008).
[2] P. Zubko, S. Gariglio, M. Gabay, P. Ghosez, and J.-M. Triscone, Annu. Rev. Condens. Matter Phys. **2**, 141 (2011).
[3] V. M. Goldschmidt, Naturwissenschaften **14**, 477 (1926).
[4] M. L. Medarde, J. Phys.: Condens. Matter **9**, 1679 (1997).
[5] T. Kimura, S. Ishihara, H. Shintani, T. Arima, K. T. Takahashi, K. Ishizaka, and Y. Tokura, Phys. Rev. B **68**, 060403(R) (2003).
[6] A. Ohtomo and H. Y. Hwang, Nature (London) **427**, 423 (2004).
[7] D. A. Dikin, M. Mehta, C. W. Bark, C. M. Folkman, C. B. Eom, and V. Chandrasekhar, Phys. Rev. Lett. **107**, 056802 (2011).
[8] L. Li, C. Richter, J. Mannhart, and R. C. Ashoori, Nat. Phys. **7**, 762 (2011).
[9] G. Cheng, M. Tomczyk, S. Lu, J. P. Veazey, M. Huang, P. Irvin, S. Ryu, H. Lee, C.-B. Eom, C. S. Hellberg, and J. Levy, Nature (London) **521**, 196 (2015).
[10] A. F. Santander-Syro, O. Copie, T. Kondo, F. Fortuna, S. Pailhès, R. Weht, X. G. Qiu, F. Bertran, A. Nicolaou, A. Taleb-Ibrahimi, P. Le Fèvre, G. Herranz, M. Bibes, N. Reyren, Y. Apertet, P. Lecoeur, A. Barthélémy, and M. J. Rozenberg, Nature (London) **469**, 189 (2011).
[11] W. Meevasana, P. D. C. King, R. H. He, S.-K. Mo, M. Hashimoto, A. Tamai, P. Songsiriritthigul, F. Baumberger, and Z.-X. Shen, Nat. Mater. **10**, 114 (2011).
[12] Z. Wang, Z. Zhong, X. Hao, S. Gerhold, B. Stoger, M. Schmid, J. Sanchez-Barriga, A. Varykhalov, C. Franchini, K. Held, and U. Diebold, Proc. Natl. Acad. Sci. USA **111**, 3933 (2014).
[13] T. C. Rödel, C. Bareille, F. Fortuna, C. Baumier, F. Bertran, P. Le Fèvre, M. Gabay, O. Hijano Cubelos, M. J. Rozenberg, T. Maroutian, P. Lecoeur, and A. F. Santander-Syro, Phys. Rev. Appl. **1**, 051002 (2014).
[14] S. McKeown Walker, A. de la Torre, F. Y. Bruno, A. Tamai, T. K. Kim, M. Hoesch, M. Shi, M. S. Bahramy, P. D. C. King, and F. Baumberger, Phys. Rev. Lett. **113**, 177601 (2014).
[15] P. D. C. King, R. H. He, T. Eknapakul, P. Buaphet, S.-K. Mo, Y. Kaneko, S. Harashima, Y. Hikita, M. S. Bahramy, C. Bell, Z. Hussain, Y. Tokura, Z.-X. Shen, H. Y. Hwang, F. Baumberger, and W. Meevasana, Phys. Rev. Lett. **108**, 117602 (2012).
[16] A. F. Santander-Syro, C. Bareille, F. Fortuna, O. Copie, M. Gabay, F. Bertran, A. Taleb-Ibrahimi, P. Le Fèvre, G. Herranz, N. Reyren, M. Bibes, A. Barthélémy, P. Lecoeur, J. Guevara, and M. J. Rozenberg, Phys. Rev. B **86**, 121107(R) (2012).
[17] C. Bareille, F. Fortuna, T. C. Rödel, F. Bertran, M. Gabay, O. H. Cubelos, A. Taleb-Ibrahimi, P. Le Fèvre, M. Bibes, A. Barthélémy, T. Maroutian, P. Lecoeur, M. J. Rozenberg, and A. F. Santander-Syro, Sci. Rep. **4**, 3586 (2014).
[18] T. C. Rödel, F. Fortuna, F. Bertran, M. Gabay, M. J. Rozenberg, A. F. Santander-Syro, and P. Le Fèvre, Phys. Rev. B **92**, 041106(R) (2015).
[19] T. C. Rödel, F. Fortuna, S. Sengupta, E. Frantzeskakis, P. Le Fèvre, F. Bertran, B. Mercey, S. Matzen, G. Agnus, T. Maroutian, P. Lecoeur, and A. F. Santander-Syro, Adv. Mater. **28**, 1976 (2016).
[20] C. Chen, J. Avila, E. Frantzeskakis, A. Levy, and M. C. Asensio, Nat. Commun. **6**, 8585 (2015).
[21] Z. Wang, S. McKeown Walker, A. Tamai, Y. Wang, Z. Ristic, F. Y. Bruno, A. de la Torre, S. Riccò, N. C. Plumb, M. Shi, P. Hlawenka, J. Sánchez-Barriga, A. Varykhalov, T. K. Kim, M. Hoesch, P. D. C. King, W. Meevasana, U. Diebold, J. Mesot, B. Moritz, T. P. Devereaux, M. Radovic, and F. Baumberger, Nat. Mater. **15**, 835 (2016).
[22] J. M. Rondinelli, S. J. May, and J. W. Freeland, MRS Bull. **37**, 261 (2012).
[23] N. Ganguli and P. J. Kelly, Phys. Rev. Lett. **113**, 127201 (2014).
[24] Z. Liao, N. Gauquelin, R. J. Green, S. Macke, J. Gonnissen, S. Thomas, Z. Zhong, L. Li, L. Si, S. Van Aert, P. Hansmann, K. Held, J. Xia, J. Verbeeck, G. Van Tendeloo, G. A. Sawatzky, G. Koster, M. Huijben, and G. Rijnders, Adv. Funct. Mater. **27**, 1606717 (2017).
[25] See Supplemental Material at http://link.aps.org/supplemental/10.1103/PhysRevB.96.041121 which includes Refs. [10,19,38–52], for further details about sample preparation, ARPES measurements, DFT calculations, and tight-binding fitting of the data.
[26] K. S. Knight, J. Alloys Compd. **509**, 6337 (2011).
[27] K. Ueda, H. Yanagi, H. Hosono, and H. Kawazoe, J. Phys.: Condens. Matter **11**, 3535 (1999).
[28] Z. Zhong and P. J. Kelly, Europhys. Lett. **84**, 27001 (2008).
[29] C. L. Jia, S. B. Mi, M. Faley, U. Poppe, J. Schubert, and K. Urban, Phys. Rev. B **79**, 081405(R) (2009).
[30] A. Rubano, C. Aruta, U. Scotti di Uccio, F. Miletto Granozio, L. Marrucci, T. Günter, T. Fink, M. Fiebig, and D. Paparo, Phys. Rev. B **88**, 245434 (2013).
[31] J. Chen, Y. Luo, X. Ou, G. Yuan, Y. Wang, Y. Yang, J. Yin, and Z. Liu, J. Appl. Phys. **113**, 204105 (2013).
[32] H. Lu, C.-W. Bark, D. Esque de los Ojos, J. Alcala, C. B. Eom, G. Catalan, and A. Gruverman, Science **336**, 59 (2012).
[33] A. Joshua, S. Pecker, J. Ruhman, E. Altman, and S. Ilani, Nat. Commun. **3**, 1129 (2012).

[34] A. Joshua, J. Ruhman, S. Pecker, E. Altman, and S. Ilani, Proc. Natl. Acad. Sci. USA **110**, 9633 (2013).
[35] H. Liang, L. Cheng, L. Wei, Z. Luo, G. Yu, C. Zeng, and Z. Zhang, Phys. Rev. B **92**, 075309 (2015).
[36] F. Trier, G. E. D. K. Prawiroatmodjo, Z. Zhong, D. V. Christensen, M. von Soosten, A. Bhowmik, J. Maria García Lastra, Y. Chen, T. S. Jespersen, and N. Pryds, Phys. Rev. Lett. **117**, 096804 (2016).
[37] G. Herranz, G. Singh, N. Bergeal, A. Jouan, J. Lesueur, J. Gázquez, M. Varela, M. Scigaj, N. Dix, F. Sánchez, and J. Fontcuberta, Nat. Commun. **6**, 6028 (2015).
[38] M. Kawasaki, A. Ohtomo, and T. Arakane, Appl. Surf. Sci. **107**, 102 (1996).
[39] S. M. Walker, F. Y. Bruno, Z. Wang, A. de la Torre, S. Riccó, A. Tamai, T. K. Kim, M. Hoesch, M. Shi, M. S. Bahramy, P. D. C. King, and F. Baumberger, Adv. Mater. **27**, 3894 (2015).
[40] H. O. Jeschke, J. Shen, and R. Valenti, New J. Phys. **17**, 023034 (2015).
[41] F. Lechermann, H. O. Jeschke, A. J. Kim, S. Backes, and R. Valenti, Phys. Rev. B **93**, 121103(R) (2016).
[42] G. Kresse and J. Furthmuller, Phys. Rev. B **54**, 11169 (1996).
[43] G. Kresse and J. Hafner, Phys. Rev. B **47**, 558 (1993).
[44] J. P. Perdew, J. A. Chevary, S. H. Vosko, K. A. Jackson, M. R. Pederson, D. J. Singh, and C. Fiolhais, Phys. Rev. B **46**, 6671 (1992).
[45] S. L. Dudarev, G. A. Botton, S. Y. Savrasov, C. J. Humphreys, and A. P. Sutton, Phys. Rev. B **57**, 1505 (1998).
[46] J. Heyd, G. E. Scuseria, and M. Ernzerhof, J. Chem. Phys. **118**, 8207 (2003).
[47] J. Paier, M. Marsman, K. Hummer, G. Kresse, I. C. Gerber, and J. G. Angyan, J. Chem. Phys. **124**, 154709 (2006).
[48] P. E. Blöchl, Phys. Rev. B **50**, 17953 (1994).
[49] G. Kresse and J. Joubert, Phys. Rev. B **59**, 1758 (1999).
[50] A. M. Glazer, Acta Crystallogr. B **28**, 3384 (1972).
[51] P. Blaha, K. Schwarz, G. K. H. Madsen, D. Kvasnicka, and J. Luitz, *WIEN2k, An Augmented Plane Wave and Local Orbitals Program for Calculating Crystal Properties* (Techn. Universität Wien, Austria, 2001).
[52] N. C. Plumb, M. Salluzzo, E. Razzoli, M. Månsson, M. Falub, J. Krempasky, C. E. Matt, J. Chang, M. Schulte, J. Braun, H. Ebert, J. Minár, B. Delley, K.-J. Zhou, T. Schmitt, M. Shi, J. Mesot, L. Patthey, and M. Radović, Phys. Rev. Lett. **113**, 086801 (2014).
[53] S. Muff, M. Fanciulli, A. P. Weber, N. Pilet, Z. Ristić, Z. Wang, N. C. Plumb, M. Radović, and J. H. Dil, Appl. Surf. Sci. (2017), doi:10.1016/j.apsusc.2017.05.229.